doi: 10.15407/ujpe62.06.0461

V.S. VASILEVSKY,[1] N.ZH. TAKIBAYEV,[2] A.D. DUISENBAY[2]

[1] Bogolyubov Institute for Theoretical Physics, Nat. Acad. of Sci. of Ukraine
(14b, Metrolohichna Str., Kyiv 03143, Ukraine; e-mail: VSVasilevsky@gmail.com)
[2] Al-Farabi Kazakh National University
(Al-Farabi Avenue 71, Almaty, 050040, Kazakhstan; e-mail: takibayev@gmail.com)

PACS 21.60.Gx, 24.10.-i

MICROSCOPIC DESCRIPTION OF ^{8}Li AND ^{8}B NUCLEI WITHIN A THREE-CLUSTER MODEL

The theoretical analysis of structures of the bound and resonance states in ^8Li and ^8B nuclei is performed within a three-cluster microscopic model. In the framework of this model, ^8Li and ^8B nuclei are considered as three-cluster configurations $^4He + ^3H + n$ and $^4He + ^3He + p$, respectively. A distinguished peculiarity of the model is that it allows us to consider the polarizability of weakly bound nuclei such as ^7Li composed of an alpha particle and a triton or ^7Be composed of an alpha particle and ^3He. Gaussian and oscillator bases are used to expand the three-cluster wave function and to represent the many-channel Schrödinger equation in a matrix form. The main attention of the present study is paid to the effects of cluster polarization on the spectrum of bound and resonance states of ^8Li and ^8B and on the elastic and inelastic $n + ^7Li$ and $p + ^7Be$ scattering. It is shown that the cluster polarization has a great impact on parameters of the bound and resonance states in ^8Li and ^8B. For instance, it decreases the energy of resonance states by 0.7–2.0 MeV and increases their lifetime by more than three times. The roles of spin-orbital and Coulomb interactions in the formation of the spectrum of excited states in nuclei ^8Li and ^8B are studied in detail. In particular, it is found out that the Coulomb forces shift up the energy of resonance states in ^8B with respect to the position of corresponding resonance states in ^8Li and increases their widths.

K e y w o r d s: cluster model, resonance state, cluster polarization.

1. Introduction

The analysis of astrophysical data on the abundance of light atomic nuclei in the Universe stimulated new and more detailed experimental and theoretical investigations of the reactions induced by the interaction of light nuclei. For the astrophysical applications, one has to know the cross-section of a reaction at the low-energy region, which amounts several keV in the entrance channel of the reaction. This energy region can be easily achieved at experimental facilities for the reactions induced by the interaction of neutrons with light nuclei. However, it is not the case for the interaction of light nuclei containing one or more protons. The Coulomb interaction between nuclei makes it very difficult to measure the cross-section. In this case, the theoretical methods are an invaluable tool to determine or to evaluate the cross-section of importance.

Since many of the light nuclei are weakly bound, they could easily change their size or shape, while interacting with neutrons, protons, or other light nuclei. This phenomenon is called the polarization. A microscopic three-cluster model was formulated in Ref. [1] to take the polarizability of interacting clusters into account. We refer to it as "cluster polarization". It was shown in Refs. [1–4] that the cluster polarization plays an important role in the formation of bound

and resonance states in seven nucleon systems. It was also shown that the cluster polarization has a large impact on the reactions of different types in ^{7}Li and ^{7}Be nuclei. It was also established that the cluster polarization has the largest impact on the structures of seven nucleon systems among other types of polarization, which have been used previously in the literature. In addition, the cluster polarization, as was demonstrated in [3, 4], increases the astrophysical S factor of the radiative capture reactions in ^{7}Li and ^{7}Be nuclei by a few times.

Within the present paper, the effects of cluster polarization will be studied in light mirror nuclei ^{8}Li and ^{8}B. We will also study how the cluster polarization affects the interaction of a neutron with ^{7}Li and a proton with ^{7}Be. Note that both ^{7}Li and ^{7}Be nuclei have well-established two-cluster structure: $^4\mathrm{He} + {}^3\mathrm{H}$ and $^4\mathrm{He} + {}^3\mathrm{He}$, respectively. This fact is taken into account in the present model. We are going to consider the bound and resonance states of mirror nuclei ^{8}Li and ^{8}B within a three-cluster microscopic model. We will consider the resonance states created by two-cluster and three-cluster configurations. These nuclei are of interest, because they are nuclei with large excess of neutrons and protons, respectively. They exhibit the halo properties, since the radius of the proton (neutron) cloud is much smaller than for the neutron (proton) cloud in bound states of ^{8}Li (^{8}B).

Properties of mirror nuclei ^{8}Li and ^{8}B have been intensively investigated in microscopic [5–14] and semimicroscopic models [15–19]. In addition, different experimental methods [20–30] were used to determine the structures of ^{8}Li and ^8B and nuclear reactions in these nuclei. In particular, new resonance states of ^{8}B have been recently discovered in [24, 28] in the elastic $^7\mathrm{Be} + \mathrm{p}$ scattering.

The novelty of our approach is that it allows us to consider cluster polarizations. This means that, within the proposed model, the size and shape of clusters are not fixed, but depend on the distance between interacting clusters. In the present case, we consider how the size of ^{7}Li(^{7}Be) is changed, when a neutron (proton) moves toward ^{7}Li(^{7}Be).

The microscopic method used in this paper pursues two goals: (1) it aims at studying the polarizability of nuclei with the distinguished cluster structure induced by the incident cluster; (2) it also aims at a more advanced description of the resonance states in three-cluster compound systems.

The paper is structured in the following way. Section 2 shortly describes the microscopic method to study the cluster polarization in light nuclei. Section 3 presents details of selecting the input parameters of calculations and the results of theoretical analysis of bound and resonance states in ^{8}Li and ^{8}B.

2. Method and Model Space

We shall consider ^{8}Li as a three-cluster configuration $^8\mathrm{Li} = \alpha + \mathrm{t} + \mathrm{n}$ and nucleus ^{8}B as the configuration $^8\mathrm{B} = \alpha + {}^3\mathrm{He} + \mathrm{p}$. These configurations are dynamically distinguished from other three-cluster configurations, since they have minimal threshold energy compared to other three-cluster configurations in ^{8}Li and ^{8}B. By using such three-cluster configurations, we can consider the following set of two-cluster channels: $^7\mathrm{Li} + \mathrm{n}$, $^5\mathrm{He} + {}^3\mathrm{H}$, $^4\mathrm{H} + {}^4\mathrm{He}$ in ^{8}Li and $^7\mathrm{Be} + \mathrm{p}$, $^5\mathrm{Li} + {}^3\mathrm{He}$, $^4\mathrm{Li} + {}^4\mathrm{He}$ in ^{8}B. Moreover, with such three-cluster configurations, we can consider nuclei ^{7}Li, ^{5}He, ^{4}H, ^{7}Be, ^{5}Li, and ^{4}Li as two-cluster systems,

$$^7\mathrm{Li} = \alpha + \mathrm{t}, \quad ^5\mathrm{He} = \alpha + \mathrm{n}, \quad ^4\mathrm{H} = \mathrm{t} + \mathrm{n},$$
$$^7\mathrm{Be} = \alpha + {}^3\mathrm{He}, \quad ^5\mathrm{Li} = \alpha + \mathrm{p}, \quad ^4\mathrm{Li} = {}^3\mathrm{He} + \mathrm{p},$$

and can provide a more advanced description of the internal structure of these nuclei.

To describe the selected three-cluster configurations, we employ the Algebraic Model with Gaussian and Oscillator Basis (AMGOB) [1–4]. Actually, this model is a matrix form of quantum theory of many-channel systems with correct boundary conditions.

We start with the construction of wave functions for two-cluster subsystems and for compound three-cluster system. For the sake of simplicity, we represent these functions in the LS coupling scheme. This scheme will be used in the calculations of the bound state spectrum. However, to study the continuous spectrum states, we use the jj coupling scheme. The two-cluster wave function $\Psi^{(\alpha)}_{J_\alpha}$, describing the interaction of clusters with indices β and γ, can be written as

$$\Psi^{(\alpha)}_{E_\alpha J_\alpha} = \widehat{\mathcal{A}}_{\beta\gamma} \left\{ \left[\Phi_\beta \left(A_\beta, s_\beta \right) \Phi_\gamma \left(A_\gamma, s_\gamma \right) \right]_{S_\alpha} \times \right.$$
$$\left. \times \, g^{(E)}_{\lambda_\alpha J_\alpha} \left(x_\alpha \right) Y_{\lambda_\alpha} \left(\widehat{\mathbf{x}}_\alpha \right) \right\}_{J_\alpha}, \qquad (1)$$

where the function $g^{(E)}_{\lambda_\alpha J_\alpha}(x_\alpha)$ represents a radial part of the wave function of the two-cluster relative motion, and the spherical harmonic $Y_{\lambda_\alpha}(\widehat{\mathbf{x}}_\alpha)$ represents

its angular part. The indices α, β, and γ form cyclic permutations of 1, 2, and 3.

The wave function of discrete and continuous spectrum states of a three-cluster system is

$$\Psi_{E,J} = \widehat{\mathcal{A}}\left\{\left[\Phi_1\left(A_1, s_1\right)\Phi_2\left(A_2, s_2\right)\Phi_3\left(A_3, s_3\right)\right]_S \times \right.$$
$$\left. \times \sum_{\alpha=1}^{3} f^{(E,J)}_{\lambda_\alpha l_\alpha, L}\left(x_\alpha, y_\alpha\right)\left\{Y_{\lambda_\alpha}\left(\widehat{\mathbf{x}}_\alpha\right) Y_{l_\alpha}\left(\widehat{\mathbf{y}}_\alpha\right)\right\}_L\right\}_J, \qquad (2)$$

where $\Phi_\alpha\left(A_\alpha, s_\alpha\right)$ is a many-particle shell-model wave function describing the internal motion of the cluster α ($\alpha = 1, 2, 3$) consisting of A_α nucleons ($1 \leq \leq A_\alpha \leq 4$), and s_α denotes the cluster spin.

Similarly to the case of three particles, we use three Faddeev amplitudes $f^{(E,J)}_{\lambda_\alpha l_\alpha, L}\left(x_\alpha, y_\alpha\right)$ and three sets of Jacobi coordinates $\mathbf{x}_\alpha$ and $\mathbf{y}_\alpha$. The Jacobi coordinates determine the relative position of the center-of-mass of three clusters. In our notations, $\mathbf{x}_\alpha$ is the Jacobi vector proportional to the distance between β and γ clusters, while $\mathbf{y}_\alpha$ is the Jacobi vector connecting the position of the cluster α with the center-of-mass of the β and γ clusters. The vectors $\widehat{\mathbf{x}}_\alpha$ and $\widehat{\mathbf{y}}_\alpha$ denote unit vectors $\widehat{\mathbf{x}}_\alpha = \mathbf{x}_\alpha / \left|\mathbf{x}_\alpha\right|$ and $\widehat{\mathbf{y}}_\alpha = \mathbf{y}_\alpha / \left|\mathbf{y}_\alpha\right|$. The antisymmetrization operators $\widehat{\mathcal{A}}_{\beta\gamma}$ and $\widehat{\mathcal{A}}$ make antisymmetric wave functions of two- and three-cluster systems, respectively. Note that the shell-model wave functions $\Phi_\alpha\left(A_\alpha, s_\beta\right)$ are antisymmetric. Thus, the operators $\widehat{\mathcal{A}}_{\beta\gamma}$ and $\widehat{\mathcal{A}}$ permute nucleons from different clusters.

For s-shell nuclei, the wave function $\Phi_\alpha\left(A_\alpha, s_\alpha\right)$ can be represented as a product of the coordinate and spin-isospin parts:

$$\Phi_\alpha\left(A_\alpha, s_\alpha\right) = \exp\left\{-\frac{1}{2}\left(\frac{\rho_\alpha}{b}\right)^2\right\}\chi_{s_\alpha}\left(A_\alpha\right), \qquad (3)$$

where

$$\rho_\alpha = \sqrt{\sum_{i\in A_\alpha}\left(\mathbf{r}_i - \mathbf{R}_\alpha\right)^2},$$

$\mathbf{r}_i$ is a single-particle coordinate of the ith nucleon, and $\mathbf{R}_\alpha = \sum_{i\in A_\alpha}\mathbf{r}_i / A_\alpha$ is the coordinate of the center-of-mass of A_α nucleons. The spin-isospin part of the wave function $\chi_{s_\alpha}(A_\alpha)$ provides the antisymmetric properties of the wave function $\Phi_\alpha(A_\alpha, s_\alpha)$ and the normalization condition $\langle\Phi_\alpha(A_\alpha, s_\alpha)|\Phi_\alpha(A_\alpha, s_\alpha)\rangle = 1$. If a cluster consists of one nucleon only, then $\rho_\alpha = 0$, and the wave function $\Phi_\alpha(A_\alpha, s_\alpha)$ of the cluster is represented by the spin-isospin function $\chi_{s_\alpha}(A_\alpha)$. The expectation value $\mathcal{E}_\alpha = \left\langle\Phi_\alpha\left(A_\alpha, s_\alpha\right)\left|\widehat{H}^{(1)}_\alpha\right|\Phi_\alpha\left(A_\alpha, s_\alpha\right)\right\rangle$ determines the internal energy of cluster α. The sum $\sum_{\alpha=1}^{3}\mathcal{E}_\alpha$ determines the three-cluster threshold energy.

One can see in Eq. (3) that the shell-model wave function $\Phi_\alpha\left(A_\alpha, s_\beta\right)$ explicitly depends on the oscillator length b. In different realizations of the many-cluster model, this parameter is used as a variational or adjustable parameter. As a rule, the oscillator length is adjusted to minimize the bound-state energy of clusters or to reproduce their size (i.e., the mass or proton root-mean-square (rms) radius). Within all our models, we use the common oscillator length for all clusters involved in calculations.

The Faddeev amplitude $f^{(E,J)}_{\lambda_\alpha l_\alpha, L}\left(x_\alpha, y_\alpha\right)$ in Eq. (2) is marked by two partial orbital momenta λ_α and l_α. They are associated with the Jacobi vectors $\mathbf{x}_\alpha$ and $\mathbf{y}_\alpha$, respectively. In what follows, we assume that λ_α is the orbital momentum of the two-cluster subsystem, and l_α is the orbital momentum connected with the rotation of the third cluster around the center-of-mass of the two-cluster subsystem.

To complete definitions, we have to determine single-, two-, and three-cluster Hamiltonians. Hamiltonian $\widehat{H}^{(1)}_\alpha$ determining the internal structure of a cluster with A_α nucleons is

$$\widehat{H}^{(1)}_\alpha = \widehat{T}_\alpha + \sum_{i<j\in A_\alpha}\widehat{V}(ij),$$

where $\widehat{T}_\alpha$ is the kinetic energy operator in the center-of-mass system, and $\widehat{V}\left(ij\right)$ is a nucleon-nucleon potential. The two-cluster Hamiltonian describing the interaction of the clusters with indices β and γ is

$$\widehat{H}^{(2)}_\alpha = \widehat{H}^{(1)}_\beta + \widehat{H}^{(1)}_\gamma + \widehat{T}_{x_\alpha} + \sum_{i\in A_\beta, j\in A_\gamma}\widehat{V}(ij),$$

and the three-cluster Hamiltonian can be represented as

$$\widehat{H} = \widehat{H}^{(2)}_\alpha + \widehat{H}^{(1)}_\alpha + \widehat{T}_{y_\alpha} +$$
$$+ \sum_{i\in A_\beta,\, j\in A_\alpha}\widehat{V}(ij) + \sum_{i\in A_\alpha,\, j\in A_\gamma}\widehat{V}(ij),$$

where

$$\widehat{T}_z = -\frac{\hbar^2}{2m}\Delta_z$$

is the kinetic energy operator associated with the Jacobi coordinate $z = x_\alpha$ or y_α. To solve correctly the three-cluster problems, we need to solve the two-cluster Schrödinger equation

$$\left(\widehat{H}^{(2)}_\alpha - E_{\sigma,\alpha}\right)\Psi^{(\alpha)}_{E_\alpha J_\alpha} = 0 \qquad (4)$$

for three different two-cluster partitions α ($\alpha = 1$, 2, 3). The energies of two-cluster bound states $E_{\sigma,\alpha}$ determine the threshold energy of two-body channels, and the wave functions $\Psi^{(\alpha)}_{E_{\alpha,\alpha},J_\alpha}$ determine the asymptotic form of three-body functions in the part of the coordinate space, which was denoted by Faddeev and Merkuriev as Ω_α (see pp. 134–135 of book [31]), i.e. in the region, where the distance x_α between a selected pair of clusters is much smaller than the distance between other pairs of clusters ($x_\alpha \ll x_\beta$, $x_\alpha \ll x_\gamma$).

Having solved the Schrödinger equations (4) for all two-cluster subsystems, we can proceed with solving the Schrödinger equation for a three-cluster system (see Eqs. (31) and (33) in Ref. [1]). It is well known [32] that the Schrödinger equations for two- and three-cluster systems can be reduced to two- and three-body equations, respectively, with nonlocal energy-dependent potentials. This needs a special attention and should be taken into account. The most simple way of overcoming this problem is to use a square-integrable basis.

The essence of the model employed in the present investigations is the application of a discretization scheme with the help of a square-integrable basis. This allows us to reduce the Schrödinger equation for the many-channel system to the system of algebraic equations, which can be easily solved numerically. In the present model, we use the Gaussian basis to describe the bound and pseudobound states of two-cluster subsystems, and we employ the oscillator basis to study the interaction of the third cluster with the two-cluster subsystem. The explicit definition of the Gauss and oscillator basis functions, derivation of a system of linear equations for the wave function, and formulation of boundary conditions for the wave function in the discrete representation are presented in Refs. [1, 2].

Before proceeding to the numerical solution of the two- and three-cluster Schrödinger equations, we need to discuss some important properties of three-cluster wave functions. In the present model, when the three-cluster system is projected onto the set of binary configurations (partitions), the three-cluster wave function turns out to be the many-component wave function, each component being associated with a binary channel c. The index c is a multiple index $c = \{E_{\sigma,\alpha}, J_\alpha, l_\alpha\}$, which is comprised of the energy $E_{\sigma,\alpha}$ and the angular momentum J_α of a "target"-two-cluster subsystem, and the orbital momentum l_α of the third cluster – "projectile". Within our model, the number of components of the three-cluster function is substantially increased as the total spin S and total orbital momentum L of the compound system are not quantum numbers. The total spin S of ^{8}Li and ^{8}B within the present model is a vector sum of the spins of ^{3}H and n and ^{3}He and p, respectively. This gives us the total spin $S = 0$ and $S = 1$. Thus, the state with total angular momentum J is created by a combination of four different values of the total orbital momentum L and the total spin S:

$$|J\rangle = |(L = J, S = 0)\rangle + |(L = J - 1, S = 1)\rangle + \\ + |(L = J, S = 1)\rangle + |(L = J + 1, S = 1)\rangle.$$

There are two exceptions from this rule. First, for the total angular momentum equal to zero, we have a combination of two LS states: $|J = 0\rangle = |(L = 0, S = 0)\rangle + |(L = 1, S = 1)\rangle$. Second, the total angular momentum $J = 1$ consists of four components

$$|J = 1\rangle = |(L = 1, S = 0)\rangle + |(L = 0, S = 1)\rangle + \\ + |(L = 1, S = 1)\rangle + |(L = 2, S = 1)\rangle$$

for positive parity states and of three components

$$|J = 1\rangle = |(L = 1, S = 0)\rangle + |(L = 1, S = 1)\rangle + \\ + |(L = 2, S = 1)\rangle$$

for negative parity states, as it is impossible to construct the wave functions of negative parity states with the zero value of the total orbital momentum L.

All four combinations (L, S) are involved in calculations of the Hamiltonian and wave functions of bound and scattering states. Moreover, these quantum numbers will be included in the collection of five quantum numbers, which unambiguously enumerate channels of the compound system $c = \{E_{\sigma,\alpha}, J_\alpha, l_\alpha, L, S\}$, provided that the quantum numbers L, S are compatible with the given value of the total angular momentum J and parity π.

3. Structure of ^{8}Li and ^{8}B

To obtain the spectrum of discrete and continuous spectrum states of ^{8}Li and ^{8}B, we use two nucleon-nucleon potentials: the Minnesota potential (MP) (central components are taken from [33], VI version of the spin-orbital component from [34]), and modified Hasegawa–Nagata potential (MHNP) from [35, 36].

The oscillator length b, which is common for all clusters, is adopted to minimize the threshold energy of the three-cluster channel. In this way, we optimize the description of the internal structure of all clusters. For the MP and the MHNP, we have $b = 1.3451$ fm and 1.362 fm, respectively.

In present calculations, we use the Majorana parameter m of the MHNP [35,36] and the parameter u of the MP [33] as adjustable ones. These parameters are slightly changed to reproduce the bound-state energy of ^{8}B. This is done in order to be consistent with the experimental situation in ^{8}Li and ^{8}B nuclei.

3.1. Bound states

In Table 1, we show the spectra of the ^{8}Li and ^{8}B bound states, which are obtained with two sets of nucleon-nucleon potentials (NNP) and with the "optimal" input parameters. Experimental data are from Ref. [20]. The energies of bound states in ^{8}Li and ^{8}B are reckoned from the two-cluster thresholds $^7\mathrm{Li} + \mathrm{n}$ and $^7\mathrm{Be} + \mathrm{n}$, respectively. One can see that the MHNP provides a more correct description of the bound state spectrum in ^{8}Li. Meanwhile, the optimal input parameters of the MP lead to a very close position of the ground 2^+ state and the first excited 1^+ state.

To achieve the convergence of the energies of the ^{8}Li and ^{8}B bound states as functions of the numbers of Gaussian and oscillator functions, we investigated in detail how the energies of bound and resonance states depend on the number of basis functions. We found that 4 Gaussian functions and 50 oscillator functions provide an acceptable precision of microscopic calculations of the energy and other parameters of the bounds states such as, for instance, the root-mean-square proton, neutron, and mass radii. It is also established that 4 Gaussian functions and 130 oscillator functions guarantee a necessary precision of the calculations of the scattering matrix and the energies and widths of resonance states.

In Table 2, we display the proton, neutron, and mass rms radii in the ground state of ^{8}Li and ^{8}B nuclei. Experimental data are taken from Ref. [23]. Theoretical results are in a good agreement with the experimental data. One can see that our results confirm the existence of the neutron halo in ^{8}Li and the proton halo in ^{8}B, as the neutron (proton) rms radius is larger than the proton (neutron) rms radius in ^{8}Li (^{8}B). This is confirmed by the last column of the Table, where the difference between the proton and neutron rms radii ΔR is displayed. Our results are also in a good agreement with the results, obtained in similar microscopic models [5, 9].

As was pointed out above, a wave function of each states (bound or unbound one) consists of four components with different values of the total orbital momentum L and total spin S. One could expects that contribution of these components to the total wave function depends on energy and value of total angular momentum J. In Table 3 we show a contribution $W(L,S)$ of states with different values of the total orbital momentum L and total spin S to the wave function of bound states in ^{8}Li and ^{8}B. The 2^+ ground state of the ^{8}Li nucleus is mainly represented by the state with $S = L = 1$, meanwhile excite 1^+ states are represented by two combinations of the total spin and total orbital momentum: $(L = 1, S = 0)$

Table 1. **Optimal input parameters and the spectrum of bound states in ^{8}Li and ^{8}B. Energies E (MeV) of the bound states are determined from the $^7\mathrm{Li} + \mathrm{n}$ and $^7\mathrm{Be} + \mathrm{p}$ thresholds in ^{8}Li and ^{8}B, respectively**

Nucleus	^{8}Li			^{8}B		
NNP	MP	MHNP	Exp.	MP	MHNP	Exp.
b, fm	1.3451	1.3620		1.3451	1.3620	
m (u)	0.9600	0.4157		0.9600	0.4157	
J^π	E					
2^+	−1.958	−1.908	−2.032	−0.1368	−0.1393	−0.1375
1^+	−1.607	−0.977	−1.051			

Table 2. **Proton (R_p), neutron (R_n), and mass (R_m) rms radii and the difference $\Delta R = \lvert R_p - R_n \rvert$ (in fm) in the ground states of ^{8}Li and ^{8}B**

Nucleus	NNP	R_p	R_n	R_m	ΔR
^{8}Li	MP	2.174	2.516	2.394	0.342
	MHNP	2.174	2.548	2.415	0.374
	Exp.	2.266 ± 0.02	2.446 ± 0.02	2.376 ± 0.02	
^{8}B	MP	2.724	2.217	2.546	0.507
	MHNP	2.756	2.244	2.576	0.512
	Exp.	2.496 ± 0.03	2.336 ± 0.03	2.436 ± 0.03	

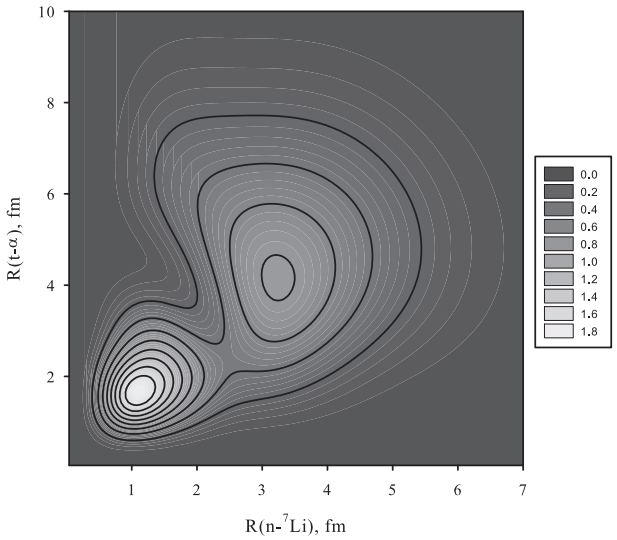

Fig. 1. Correlation function of the ^{8}Li ground state as a function of the distances between ^{3}H and ^{4}He clusters and between neutron and ^{7}Li

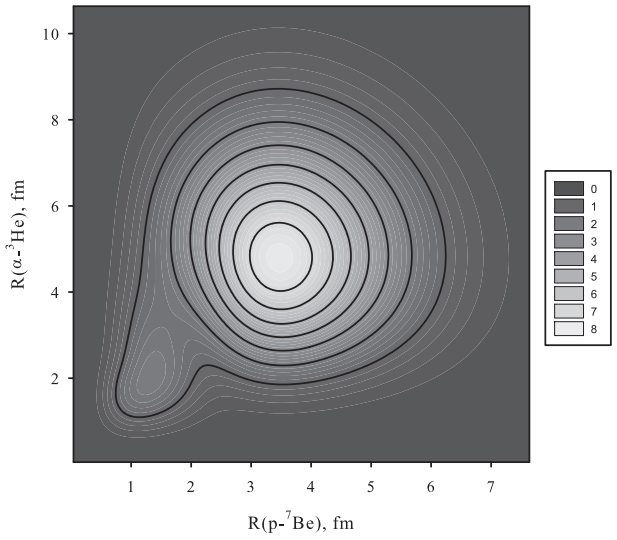

Fig. 2. Correlation function of the ^{8}B ground state as a function of distances between ^{3}He and ^{4}He clusters and between proton and ^{7}Be

and $(L = 1, S = 1)$. There is a negligible small contribution of the state $(L = 3, S = 1)$ to the wave function of the 2^+ ground state and contribution of the state $(L = 0, S = 1)$ to the wave function of the 1^+ excited states. Presented results are obtained with the Minnesota potential, and they are close to results obtained with the MHNP. As we see that the wave function of the 2^+ bound state in ^{8}B and wave function of that state in ^{8}Li is mainly represented by component $(L = 1, S = 1)$. The weight of this component is more than 92%. It is interesting to note that the structure of the 2^+ bound states in terms of $W(L, S)$ in ^{8}Li and ^{8}B is similar despite that the 2^+ bound state in ^{8}Be is weakly bound contrary to the 2^+ state in ^{8}Li. Table 3 demonstrates that the spin-orbital components of the nucleon-nucleon forces play an important role in formation of bound states in ^{8}Li and ^{8}B.

The wave functions of bound states allow us to study the structure and peculiarities of ^{8}Li and ^{8}B in these states. First, we can calculate the probability distribution of relative positions of interacting clusters. In Fig. 1, we display a correlation function (see the definition in Ref. [1]) for the ground 2^+ state in ^{8}Li, which is calculated with the MP. This figure indicates that the most probable configuration of the ^{8}Li ground state is an acute triangle with a base ≈1.8 fm (the distance between ^{3}H and ^{4}He forming ^{7}Li) and a height ≈1.2 fm (remoteness of a neutron from ^{7}Li nuclei). There is also the second maximum in Fig. 1, which corresponds to a very dispersed three-cluster configuration with the distance between clusters ^{3}H and ^{4}He more than 4 fm and the n+^{7}Li distance exceeding 3 fm. However, the probability for the compact configuration is approximately two times smaller than for the "principal" configuration. These dominant configurations justify the existence of a neutron halo in ^{8}Li.

The correlation function for the 2^+ ground state in ^{8}B presented in Fig. 2 shows that the ^{8}B ground state is more dispersed in space than the ground state of ^{8}Li. Indeed, the most probable distance between ^{3}H and ^{4}He is approximately 5 fm, and the distance between a proton and ^{7}Be is more than 3 fm. Such form of the triangle is due to the Coulomb interac-

Table 3. **Weight $W(L, S)$ of LS states in the wave function of bound states in ^{8}Li and ^{8}B**

Nucleus	^{8}Li			^{8}B
J^π	2^+	1^+	1^+	2^+
E, MeV	–2.011	–1.926	–0.461	–0.137
$W(J, 0)$	2.29	80.52	16.62	3.72
$W(0, 1)$		0.05	0.27	
$W(1, 1)$	95.07	15.75	82.94	92.91
$W(2, 1)$	2.62	3.69	0.17	3.31
$W(3, 1)$	0.02			0.06

tion, which reduces the bound-state energy from –1.908 MeV in ^{8}Li to –0.139 MeV in ^{8}B.

3.2. Resonance states and $n+^7Li$ and $p+^7Be$ scattering

Let us now turn our attention to the resonance states. Resonance states in ^{8}Li and ^{8}B, generated by the interaction of a neutron with ^{7}Li and a proton with ^{7}Be, respectively, are demonstrated in Tables 4 and 5. Experimental parameters of resonance states are taken from Ref. [20]. As one can see, the energies and widths of resonance states strongly depend on the shape of a nucleon-nucleon potential. For instance, the energy of the first 3^+ resonance state in ^{8}Li obtained with the MHNP potential is 12 times larger than one calculated with the MP, and the width is almost 50 times larger than the width calculated with the MP. There is one exception where the parameters of a resonance state calculated with both potentials are very close to each other. This is the 3^+ resonance state in ^{8}B. In this case, the energies and widths of the resonance states do not differ so dramatically, as for other resonance states.

Comparing the theoretical and experimental parameters of resonance states, we come to the conclusion that the MHNP provides a more precise description of resonance states of ^{8}Li and ^{8}B than the MP. One can see from Tables 4 and 5, the energies and widths of the 1^+ and 2^- resonance states of ^{8}B and the 1^+ resonance state of ^{8}Li calculated with the MHNP are close to experimental values. However, the MP provides a fairly good description of parameters of the 4^+ resonance state of ^{8}Li and 3^+ resonance state of ^{8}B.

3.3. Effect of cluster polarization

The above-mentioned results are obtained with taking the cluster polarization into account. To see explicitly the effects of the cluster polarization, the polarizability of clusters is switched-off. We demonstrate the effects of the cluster polarization only for two bound states and two resonance states determined with the MHNP. By switching-off the cluster polarization in ^{8}Li, we obtain the energies of the bound states $E(2+) = -1.247$ MeV and $E(1+) = -0.538$ MeV, which should be compared with $E(2^+) = -2.001$ MeV and $E(1^+) = -1.308$ MeV. As we see, the cluster polarization decreases significantly the energies of the bound states in ^{8}Li. Let us turn our attention to the resonance states. Note that the most part of resonance states of ^{8}Li (^{8}B) displayed in Tables 4 and 5 are determined in the $^7\mathrm{Li}+\mathrm{n}$ ($^7\mathrm{Be}+\mathrm{p}$) elastic scatter-

Table 4. **Spectrum of resonance states in ^{8}Li. Energies of resonances are given in MeV (Theory) or in MeV ± keV (Experiment). Theoretical and experimental widths of resonance states are indicated in keV**

^{8}Li				
J^π		MP	MHNP	Exp.
3^+	E	0.049	0.610	0.223 ± 3
	Γ	3.472	165.68	33 ± 6
1^+	E	1.5351	1.002	1.178
	Γ	826.50	1433.45	≈1000
1^+	E	4.6194	2.129	3.368
	Γ	21.81	912.54	≈650
3^+	E	2.4580	3.625	
	Γ	2635.50	760.30	
4^+	E	4.486	3.190	4.498 ± 20
	Γ	63.997	1.84	35 ± 15
2^-	E		3.494	
	Γ		365.17	

Table 5. **Spectrum of resonance states in ^{8}B. Energies of resonances are given in MeV (Theory) or in MeV ± keV (Experiment). Theoretical and experimental widths of resonance states are indicated in keV**

^{8}B				
J^π		MP	MHNP	Exp.
3^+	E	2.480	2.560	2.183 ± 20
	Γ	495.09	572.14	350 ± 30
1^+	E	0.090	0.615	0.632 ± 2.5
	Γ	0.40	43.70	35.6 ± 0.6
1^-	E	1.441	1.132	
	Γ	989.38	1827.79	
0^+	E	1.644	1.128	
	Γ	870.34	299.01	
2^-	E	4.209	3.363	3.363 ± 500
	Γ	631.72	4142.80	8000 ± 4000

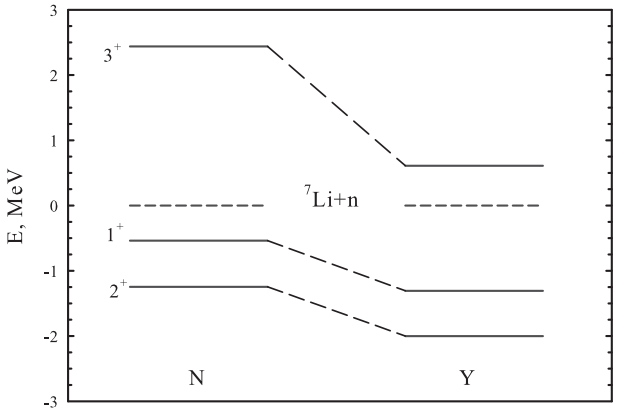

Fig. 3. Spectrum of two bound states and one resonance state of ^{8}Li obtained without (N) and with (Y) the cluster polarization

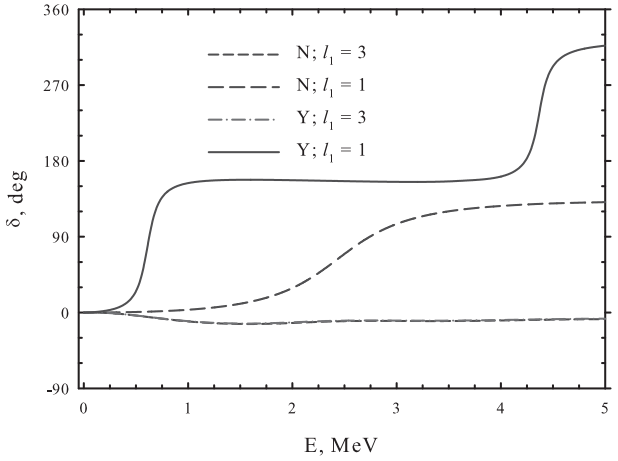

Fig. 4. Phase shifts of n $+^7$ Li scattering with the total angular momentum $J^\pi = 3^+$

ing. Consider the 1^+ resonance state of ^{8}B. By neglecting the cluster polarization, we obtain the parameters of the resonance state: $E = 0.940$ MeV and $\Gamma = 163$ keV. Comparing these parameters with the corresponding results in Tables 4 and 5, we come to the conclusion that the cluster polarization decreases 1.5 times the energy and almost 4 times the total width of the 1^+ resonance state. Stronger effects of the cluster polarization are observed in the 3^+ resonance state of ^{8}Li. The energy of the resonance state is decreased from 2.4380 MeV to 0.610 MeV, and the width is reduced from 1227 keV to 166 keV due to the cluster polarization.

Figs. 3 and 4 show effects of the cluster polarization on the scattering of neutrons from the ^{7}Li. These

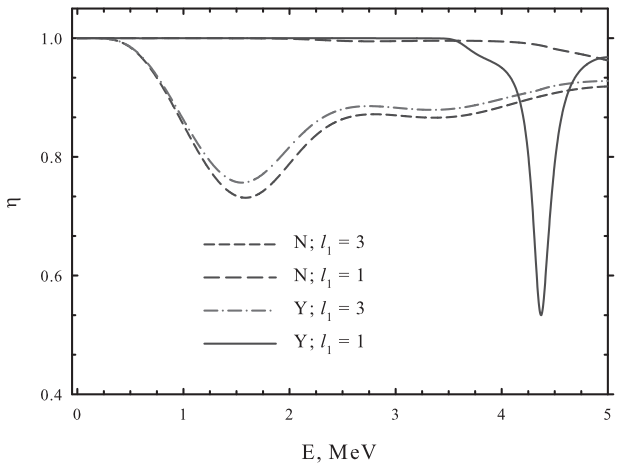

Fig. 5. Inelastic parameters of the n $+^7$ Li scattering with the total angular momentum $J^\pi = 3^+$

results are obtained with the MHNP. In Fig. 4, the orbital momentum l_1 denotes the orbital momentum of a neutron with respect to ^{7}Li nucleus. One can see that the cluster polarization influences significantly the phase shift δ of the n $+^7$ Li scattering with the orbital momentum of a neutron $l_1 = 1$. However, the effects of the cluster polarization on the n+^{7}Li scattering with $l_1 = 3$ are very small. As for the inelastic parameters η, the effects of the cluster polarization are more pronounced (see Fig. 5) than for the phase shifts of the n+^{7}Li scattering.

It is worth to note that, by solving the system of dynamic equations for continuous spectrum states, we obtain a full set of matrix elements $S_{c,\widetilde{c}}$ of the scattering S-matrix. The indices c and $\widetilde{c}$ enumerate channels of the compound system. The obtained S-matrix contains the complete information about all elastic and inelastic processes in the system. We use two different parametrizations of the S-matrix in order to analyze the dynamics of the processes and to determine important physical quantities such as the total and partial widths of resonance states. In the first representation, the complex S-matrix is expressed through the real phase shifts $\delta_{c,\widetilde{c}}$ and inelastic parameters $\eta_{c,\widetilde{c}}$

$$S_{c,\widetilde{c}} = \eta_{c,\widetilde{c}} \exp\{2i\delta_{c,\widetilde{c}}\}.$$

Usually, we analyze only the diagonal ($c = \widetilde{c}$) phase shifts and inelastic parameters, as was shown in Figs. 3 and 4. These quantities allow us to study the general properties of elastic and inelastic processes. To obtain the S-matrix in the second representation,

we need to reduce this matrix to the diagonal form, which is called the representation of eigenchannels or representation of effective uncoupled channels. We use this representation to determine the total and partial widths of compound systems (for more details, see Ref. [37]).

There is another way for the visualization of a cluster polarization. As was suggested in [1], we can calculate how the average distance between two selected clusters depends on the distance to the third cluster, by using the wave function of a bound state of the compound system. For instance, we can calculate the average distance $R(^7Li = \alpha + t)$ ($R(^7Be = \alpha + {}^3He)$) between an alpha particle and a triton (^3He) as a function of the distance $R(n - {}^7Li)$ ($R(p - {}^7Be)$), when a neutron (proton) is moving toward ^7Li (^7Be). This quantity is displayed in Fig. 6 for the ground 2^+ and first excited 1^+ states of ^8Li. When a neutron is far away from ^7Li, the average distance between an alpha particle and a triton is approximately 4.5 fm. When a neutron approaches ^7Li, the average distance is reduced slightly, and then it is significantly stretched, if the distance $R(n - {}^7Li)$ is between 1.5 and 9 fm. It seems that, for such distances $R(n - {}^7Li)$, nucleus ^7Li changes its orientation with respect to a neutron, which results in such tremendous size of the system $\alpha + t$. Finally, when a neutron is very close to the center-of-mass of ^7Li, it is compressed to a minimal size of 1.6 fm. Thus, this figure demonstrates that ^7Li as a two-cluster system is strongly affected by the incident neutron. A somewhat different picture is observed for the ground state of ^8B. The effect of the incident proton on the distance between an alpha particle and ^3He is demonstrated in Fig. 7. The incident proton gradually decreases the size of ^7Be, which is due to a combination of the nuclear forces and the Coulomb interaction. The "phase transition" observed in bound states of ^8Li in a wide range of distances $R(n - {}^7Li)$ now takes place in a very small range of $R(p - {}^7Be)$ distances. However, the amplitude of the "phase transition" in ^8B is much more than in ^8Li. It should be noted that, without polarization, all curves in Figs. 6 and 7 are transformed into planar lines, i.e., the two-cluster subsystem radius is independent of the position of the third cluster when the polarization is neglected.

It was pointed out at the beginning of the paper that many different methods have been used to study the structure of ^8Li and ^8B. To show the consistence

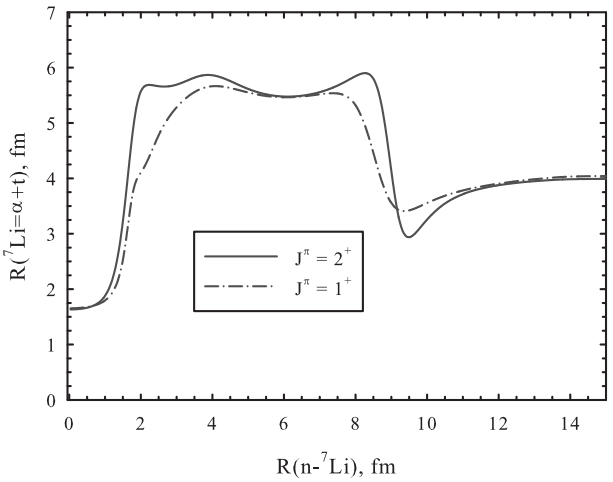

Fig. 6. Average distance between α particle and a triton as a function of the distance between a neutron and ^7Li. Calculations are made with the MHNP

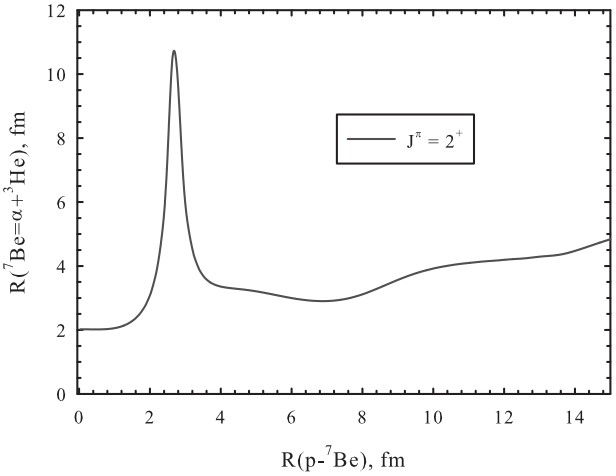

Fig. 7. Dependence of the average distance between an alpha particle and ^3He on the distance to a proton. Results are obtained with the MHNP

of our model with other models, we compare our results with those obtained by Csótó within a microscopic three-cluster model, which uses the analytic continuation to the complex plane to determine a resonance pole of the S-matrix. Both methods involve the same part of the total Hilbert space and make use of the same nucleon-nucleon potential, namely, the MHNP. The main difference of the methods is related to the way to determine the resonance parameter. In addition, the model by Csótó does not take the cluster polarization into account. In Table 6,

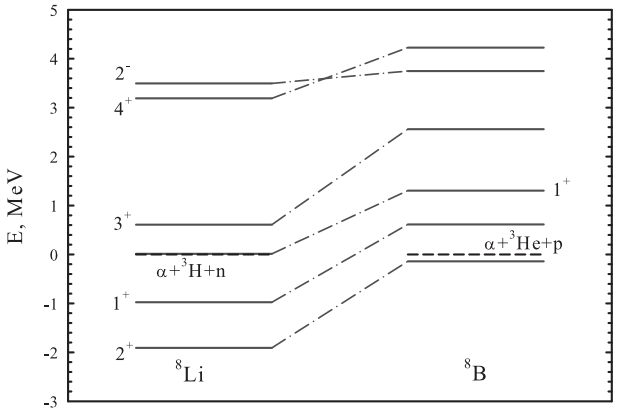

Fig. 8. Effects of the Coulomb forces on the positions of resonance states in ^{8}Li and ^{8}B

Table 6. **Low-energy spectrum of ^{8}B and ^{8}Li obtained by different methods. The energy and width are in MeV**

Nucleus	J^π	Csótó [6]		AMGOB	
		E	Γ	E	Γ
^{8}B	2^+	−0.215		−0.139	
	1^+	0.632	0.034	0.615	0.044
	1^+	1.278	0.564	1.305	0.600
	3^+	2.98	0.808	2.560	0.572
	1^+	4.33	1.5		
^{8}Li	2^+	−2.021		−1.908	
	1^+	−0.975		−0.977	
	1^+	0.037	0.006	0.014	0.002
	3^+	0.937	0.327	0.610	0.166
	1^+	2.29	1.0	2.129	0.913

Table 7. **Spectrum of resonance states in ^{8}B calculated with the MP and MHNP potentials and compared with new experimental data. The energy and width are in MeV**

J^π	Experiment		Theory			
	[24, 28]		MP		MHNP	
	E	Γ	E	Γ	E	Γ
1^+	0.630(4)	0.027(6)	0.090	0.0004	0.615	0.044
0^+	1.76(1)	$0.53^{+0.6}_{-0.1}$	1.644	0.870	1.128	0.299
3^+	2.17(2)	0.33(3)	2.480	0.495	2.560	0.572
2^+	2.36(4)	0.27(4)	1.710	1.760	3.321	1.139
1^+	3.16(2)	3.2(9)	1.372	0.842	1.305	0.600

we compare our results (marked as AMGOB) with results obtained by Csótó [6]. It is difficult to determine the exact values of parameters of the NN potential, which was used by Csótó. The differences in parameters of the resonance states can be ascribed to effects of the cluster polarization. The results collected in Table 6 indicate that our model is consistent with other three-cluster models.

3.4. Effects of Coulomb forces

Let us now consider how the Coulomb interaction affects the spectrum of bound and resonance states in the mirror nuclei ^{8}Li and ^{8}B. As we saw above (see, e.g., Table 3), the Coulomb interaction diminishes the number of bound states of ^{8}B with respect to ^{8}Li. Thus, the effective interaction between clusters is reduced by the Coulomb interaction, and this results in decreasing the energy of the 2^+ ground state and moving the 1^+ excited state up to the continuous spectrum (i.e., transforming the 1^+ bound state into a resonance state). More interesting and intriguing is the influence of the Coulomb forces on the energies and widths of resonance states. As was shown in Ref. [38], the effects of the Coulomb forces on resonance states even in two-cluster systems are not trivial. Here, we deal with the three-cluster system projected onto a set of two-cluster channels. In Fig. 8, we compare the spectrum of bound and resonance states of ^{8}Li and ^{8}B calculated with the MHNP. The dot-dashed lines connect the states with the same value of the total angular momentum J and parity π. We can see that the Coulomb interaction shifts the energies of all bound and resonance states. The effects of the Coulomb interaction are the same for all states, except for the 3^+ and 2^- resonance states. As we can see, the 2^- state has the smallest impact of the Coulomb interaction on its energy, while the largest impact is observed for the 3^+ resonance state. The main result of our consideration is that the Coulomb forces substantially increase the widths of resonance states of ^{8}B relative to the corresponding resonance states of ^{8}Li.

3.5. Theory and new experiments

In the previous sections, we compared our results with the available experimental data. It was done both for bound and resonance states. We used the classical or well-established experimental data from

Ref. [20]. Recently, Mitchell et al. in [28] presented the new results on resonance states of ^{8}B obtained by studying the $p + {}^7$Be scattering. New resonance states have been discovered in [28] and in work [24]. These results are presented in Table 7, where we compare them with our results.

Our results confirm the existence of the 0^+ resonance state in ^{8}B. Moreover, the energy and width of the resonance state calculated with the MP are close to the results by Mitchell et al. [28]. However, the parameters of the 3^+ and second 1^+ resonance states differ considerably from the new experimental results.

4. Conclusions

We have applied a three-cluster microscopic model to studying the structure of bound and resonance states of ^{8}Li and ^{8}B and the elastic and inelastic $n + {}^7$Li and $p + {}^7$Be scatterings. The model involves the polarizability of interacting clusters. It is demonstrated that the cluster polarization has a large impact on the properties of bound and resonance states and on the elastic scattering of a neutron on ^{7}Li and a proton on ^{7}Be. The present model provides a fairly good description of the bound and resonance states in mirror nuclei ^{8}Li and ^{8}B. We have investigated the effects of the spin-orbital and Coulomb forces on the structure of bound and resonance states.

This work is partially supported by the Ministry of Education and Sciences of the Republic of Kazakhstan, the Research Grant IPS 3106/GF4.

1. V.S. Vasilevsky, F. Arickx, J. Broeckhove, and T.P. Kovalenko. A microscopic three-cluster model with nuclear polarization applied to the resonances of ^{7}Be and the reaction ^{6}Li(p,^{3} He)^{4}He. *Nucl. Phys. A* **824**, 37 (2009).
2. A.V. Nesterov, V.S. Vasilevsky, T.P. Kovalenko. Effect of cluster polarization on the spectrum of the ^{7}Li nucleus and on the reaction ^{6}Li(n,^{3} H)^{4}He. *Phys. Atom. Nucl.* **72**, 1450 (2009).
3. A.V. Nesterov, V.S. Vasilevsky, T.P. Kovalenko. Microscopic model of the radiative capture reactions with cluster polarizability. Application to ^{7}Be and ^{7}Li. *Ukr. J. Phys.* **56**, No. 7, 645 (2011).
4. V.S. Vasilevsky, A.V. Nesterov, T.P. Kovalenko. Three-cluster model of radiative capture reactions in seven-nucleon systems. Effects of cluster polarization. *Phys. Atom. Nucl.* **75**, No. 7, 818 (2012).
5. A. Csótó. Proton skin of ^{8}B in a microscopic model. *Phys. Lett. B* **315**, 24 (1993).
6. A. Csótó. Low-lying continuum structures in ^{8}B and ^{8}Li in a microscopic model. *Phys. Rev. C* **61**, 024311 (2000).
7. A. Csótó. Role of spectroscopic factors in the potential-model description of the ^{7}Be$(p,\gamma)^8$B reaction. *Phys. Rev. C* **61**, 037601 (2000).
8. K. Varga, Y. Suzuki, I. Tanihata. Microscopic four-cluster description of the mirror nuclei ^{9}Li and ^{9}C, *Phys. Rev. C* **52**. 3013 (1995).
9. D. Baye, P. Descouvemont, N.K. Timofeyuk. Matter densities of ^{8}B and ^{8}Li in a microscopic cluster model and the proton-halo problem of ^{8}B. *Nucl. Phys. A* **577**, 624 (1994).
10. P. Descouvemont, D. Baye. Microscopic study of the ^{7}Li(n, γ)^{8}Li and ^{7}Be(p, γ)^{8}B reactions in a multiconfiguration three-cluster model. *Nucl. Phys. A* **567**, 341 (1994).
11. K. Varga, Y. Suzuki, I. Tanihata. Microscopic multicluster description of the ^{7}Li–^{7}Be, ^{8}Li–^{8}B and ^{9}Li–^{9}C mirror nuclei. *Nucl. Phys. A* **588**, 157 (1995).
12. P. Descouvemont, D. Baye. Quadropole excitation of ^{8}Li in a microscopic three-cluster model. *Phys. Lett. B* **292**, 235 (1992).
13. H. Stöwe, W. Zahn. Microscopic calculations for the ^{8}Li system. *Nucl. Phys. A* **289**, 317 (1977).
14. H. Stöwe and W. Zahn. Calculated excitation functions and integrated cross sections for the reactions ^{7}Li$(n, n)^7$Li and ^{7}Li$(n, n')^7$Li*. *J. Phys. G, Nucl. Phys.* **4**, 1423 (1978).
15. L.V. Grigorenko, B.V. Danilin, V.D. Efros, N.B. Shul'gina, M.V. Zhukov. Structure of the ^{8}Li and ^{8}B nuclei in an extended three-body model and astrophysical S_{17} factor. *Phys. Rev. C* **57**, 2099 (1998).
16. L.V. Grigorenko, B.V. Danilin, V.D. Efros, N.B. Shul'gina, M.V. Zhukov. Extended three-cluster model with two-cluster long-range correlations: Application to the ^{8}Li, ^{8}B nuclei. *Phys. Rev. C* **60**, 044312 (1999).
17. D. Halderson. Reactions in the ^{8}B and ^{8}Li compound systems, *Phys. Rev. C* **73**, 024612 (2006).
18. G. Kim, R.R. Khaydarov, I.-T. Cheon, F.A. Gareev. Dipole and quadrupole moments of mirror nuclei ^{8}B and ^{8}Li. *Nucl. Phys. A* **679**, 304 (2001).
19. S.B. Igamov, R. Yarmukhamedov. Asymptotic normalization coefficients (nuclear vertex constants) for $p + {}^7$ Be $\rightarrow$ $\rightarrow$ ^{8}B and the direct ^{7}Be$(p,\gamma)^8$B astrophysical S factors at solar energies. *Phys. Atom. Nucl.* **71**, 1740 (2008).
20. D.R. Tilley, J.H. Kelley, J.L. Godwin, D.J. Millener, J.E. Purcell, C.G. Sheu, H.R. Weller. Energy levels of light nuclei $A = 8$, 9, 10. *Nucl. Phys. A* **745**, 155 (2004).
21. F. Ajzenberg-Selove. Energy levels of light nuclei $A = 5$–10. *Nucl. Phys. A* **490**, 1 (1988).
22. F. Ajzenberg-Selove. Energy levels of light nuclei $A = 5$–10. *Nucl. Phys. A* **413**, 1 (1984).
23. M.M. Obuti, T. Kobayashi, D. Hirata, Y. Ogawa, A. Ozawa, K. Sugimoto, I. Tanihata, D. Olson, W. Christie, H. Wieman. Interaction cross section and interaction radius of the ^{8}B nucleus. *Nucl. Phys. A* **609**, 74 (1996).
24. J.P. Mitchell, G.V. Rogachev, E.D. Johnson, L.T. Baby, K.W. Kemper, A.M. Moro, P.N. Peplowski, A. Volya,

I. Wiedenhöver. Low-lying states in ^{8}B. *Phys. Rev. C* **82**, 011601 (2010).
25. Y. Nagai, M. Igashira, T. Takaoka, T. Kikuchi, T. Shima, A. Tomyo, A. Mengoni, T. Otsuka. ^{7}Li(n,γ)^{8}Li reaction and the S_{17} factor at $E_{\rm c.m.} > 500$ keV. *Phys. Rev. C* **71**, 055803 (2005).
26. M. Bhattacharya and E.G. Adelberger, Reanalysis of $\alpha+\alpha$ scattering and the β-delayed α spectra from ^{8}Li and ^{8}B decays. *Phys. Rev. C* **65**, 055502 (2002).
27. H. Yamaguchi, Y. Wakabayashi, S. Kubono, G. Amadio, H. Fujikawa, T. Teranishi, A. Saito, J.J. He, S. Nishimura, Y. Togano, Y.K. Kwon, M. Niikura, N. Iwasa, K. Inafuku, L.H. Khiem. Low-lying non-normal parity states in ^{8}B measured by proton elastic scattering on ^{7}Be. *Phys. Lett. B* **672**, 230 (2009).
28. J.P. Mitchell, G.V. Rogachev, E.D. Johnson, L.T. Baby, K.W. Kemper, A.M. Moro, P. Peplowski, A.S. Volya, I. Wiedenhöver. Structure of ^{8}B from elastic and inelastic ^{7}Be + p scattering. *Phys. Rev. C* **87**, 054617 (2013).
29. C. Angulo, P. Descouvemont, M. Cogneau, M. Couder, M. Gaelens, P. Leleux, M. Loiselet, G. Ryckewaert, G. Tabacaru, F. Vanderbist, T. Davinson, M. Azzouz, D. Baye, A. di Pietro, P. Figuera, R.G. Pizzone, F. de Oliveira Santos, N. de Séréville. The elastic scattering ^{7}Be + p at low energies: implications on the ^{7}Be(p, γ)^{8}Be S-factor. *Nucl. Phys. A* **719**, 300 (2003).
30. C. Angulo, M. Azzouz, P. Descouvemont, G. Tabacaru, D. Baye, M. Cogneau, M. Couder, T. Davinson, A. di Pietro, P. Figuera, M. Gaelens, P. Leleux, M. Loiselet, A. Ninane, F. de Oliveira Santos, R. G. Pizzone, G. Ryckewaert, N. de Séréville, F. Vanderbist. Experimental determination of the ^{7}Be + p scattering lengths. *Nucl. Phys. A* **716**, 211 (2003).
31. L.D. Faddeev, S.P. Merkuriev. *Quantum Scattering Theory for Several Particle Systems* (Kluwer, 1993).
32. K. Wildermuth, Y. Tang. *A Unified Theory of the Nucleus* (Vieweg, 1977).
33. D.R. Thompson, M. LeMere, Y.C. Tang. Systematic investigation of scattering problems with the resonating-group method. *Nucl. Phys. A* **286**, No. 1, 53 (1977).
34. I. Reichstein, Y.C. Tang. Study of $N+\alpha$ system with the resonating-group method. *Nucl. Phys. A*, **158**, 529 (1970).
35. A. Hasegawa, S. Nagata. Ground state of ^{6}Li. *Prog. Theor. Phys.* **45**, 786 (1971).
36. F. Tanabe, A. Tohsaki, R. Tamagaki. $\alpha\alpha$ scattering at intermediate energies. *Prog. Theor. Phys.* **53**, 677 (1975).
37. J. Broeckhove, F. Arickx, P. Hellinckx, V.S. Vasilevsky, A.V. Nesterov. The ^{5}H resonance structure studied with a three-cluster J-matrix model. *J. Phys. G Nucl. Phys.* **34**, 1955 (2007).
38. N.Z. Takibayev. Nature of Coulomb shifts of nuclear scattering resonances. *Phys. Atom. Nucl.* **68**, 1147 (2005).

Received 14.10.16

В.С. Василевський, Н.Ж. Такібаєв, А.Д. Дуйсенбай

МІКРОСКОПІЧНИЙ ОПИС ЯДЕР ^{8}Li ТА ^{8}B У РАМКАХ ТРИКЛАСТЕРНОЇ МОДЕЛІ

Р е з ю м е

У рамках трикластерної моделі виконано теоретичний аналіз структури зв'язаних та резонансних станів ядер ^{8}Li і ^{8}B. В цій моделі ядро ^{8}Li розглядається як трикластерна конфігурація ^{4}He + ^{3}H + n, а ядро ^{8}B – як конфігурація ^{4}He + ^{3}He + p. Особливість даної моделі полягає у тому, що вона дає можливість враховувати поляризовність слабкозв'язаних ядер, таких як ядро ^{7}Li, яке складається із альфа-частинки і тритона, або ядро ^{7}Be, яке складається із альфа-частинки і ^{3}He. Гаусівський та осциляторний базиси використовуються для розкладу трикластерної хвильової функції та для представлення у матричній формі рівняння Шредінгера для багатоканальної системи. Головна увага даних досліджень приділяється впливу кластерної поляризації на спектр зв'язаних та резонансних станів ядер ^{8}Li і ^{8}B та на пружне і непружне розсіяння n + ^{7}Li і p + ^{7}Be. Показано, що кластерна поляризація має великий вплив на параметри зв'язаних та резонансних станів ядер ^{8}Li і ^{8}B. Наприклад, вона зменшує енергію резонансних станів на 0,7–2,0 МеВ та збільшує їх час життя більш ніж у три рази. Детально досліджена роль спін-орбітальної та кулонівської взаємодій у формуванні спектра збуджених станів ядер ^{8}Li і ^{8}B. Зокрема, виявлено, що кулонівські сили зсувають вгору енергію резонансних станів в ядрі ^{8}B по відношенню до положень відповідних резонансних станів в ^{8}Li, а також збільшують їх ширину.